Hierarchically Structured Materials from Block Polymer Confinement within Bicontinuous Microemulsion-Derived Nanoporous Polyethylene

Brad H. Jones[†] and Timothy P. Lodge[†,‡,*]

[†]Department of Chemical Engineering and Materials Science and [‡]Department of Chemistry, University of Minnesota, Minneapolis, Minnesota 55455, United States

ABSTRACT The self-assembly behavior of block polymers under strong two-dimensional and three-dimensional confinement has been well-studied in the past decade. Confinement effects enable access to a large suite of morphologies not typically observed in the bulk. We have used nanoporous polyethylene, derived from a polymeric bicontinuous microemulsion, as a novel template for the confinement of several different cylinder-forming block polymer systems: poly(isoprene-*b*-2-vinylpyridine), poly(styrene-*b*-isoprene), and poly(isoprene-*b*-dimethylsiloxane). The resultant materials exhibit unique hierarchical arrangements of structure with two distinct length scales. First, the polyethylene template imparts a disordered, microemulsion-like periodicity between bicontinuous polyethylene and block polymer networks with sizes on the order of 100 nm. Second, the block polymer networks display internal periodic arrangements produced by the spontaneous segregation of their incompatible constituents. The microphase-separated morphologies observed are similar to those previously reported for confinement of block polymers in cylindrical pores. However, at present, the morphologies are spatially variant in a complex manner, due to the three-dimensionally interconnected nature of the confining geometry and its distribution in pore sizes. We have further exploited the unique structure of the polyethylene template to generate new hierarchically structured porous monoliths. Poly(isoprene-*b*-2-vinylpyridine) is used as a model system in which the pyridine block is cross-linked, post-infiltration, and the polyethylene template is subsequently extracted. The resultant materials possess a three-dimensionally continuous pore network, of which the pore walls retain the unique, microphase-separated morphology of the confined block polymer.

KEYWORDS: hierarchically structured materials · confinement of block polymers · nanoporous polyethylene · bicontinuous microemulsion · template

Researchers have expended substantial effort in recent years to develop synthetic routes and processing strategies for the preparation of hierarchically structured materials.[1−4] Such materials exhibit multiple levels of structural organization existing simultaneously over disparate length scales. Their efforts have often been motivated by hierarchical structures occurring in nature that confer unique functional properties to the host organism. For example, the discoveries of hierarchical surface textures on the leaves of various plant species[5,6] and the feet of gecko[7−10] have spawned intense activity toward the development of synthetic analogues, having potential application as water-repellant[11−17] and dry adhesive materials,[18−22] respectively. Block polymers offer many attractive possibilities in the design of new hierarchically structured monolithic materials. The familiar suite of microphase-separated morphologies, readily accessible through control of block chemistry, molecular architecture, and block length, can be utilized to provide spontaneous structural organization over roughly mesoscopic (2−50 nm) length scales.[23−27] Moreover, the selective voiding of domains formed by a specific block(s) through simple chemical etching can afford nanoporous materials with uniform pore shapes and sizes;[28,29] such materials have potential in many advanced applications, including catalysis,[30] separations and drug delivery,[31] and electronic devices.[32] Several strategies have been employed to impart hierarchical organization into block polymer-based materials at length scales differing by nearly an order of magnitude or more, typically through the simultaneous or sequential exploitation of multiple phase separation or segregation processes.[33−48]

At present, we report hierarchically structured polymeric materials obtained through an alternative route—by confinement of block polymers within a predefined rigid template. The confinement of block polymers has been extensively studied in the past decade, both from a fundamental perspective and as a novel route to functional materials.[49] Confinement effects can be used to access a large catalogue of microphase-separated morphologies that are distinctly different from their bulk counterparts. The equilibrium morphology of a confined block polymer is critically linked

* Address correspondence to lodge@umn.edu.

Received for review August 12, 2011 and accepted October 3, 2011.

Published online October 12, 2011
10.1021/nn203096x

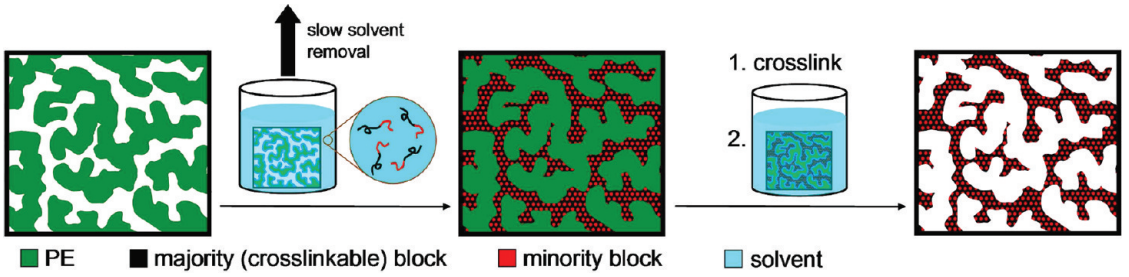

Figure 1. General templating route employed to hierarchically structured polymeric materials. The pores of nanoporous PE having a BμE structure are infiltrated by capillary action with a concentrated solution of diblock copolymer (or diblock copolymer/homopolymer blend). The solvent is slowly removed to self-assemble the copolymer and maximize the pore filling of the template. Hierarchically structured polymeric material is obtained having BμE-like periodicity between domains of PE and copolymer and microphase separation within the latter domains. In one model copolymer system, the majority block is cross-linked and the PE template is subsequently removed by selective solvation. The resultant material possesses a three-dimensionally continuous pore network with microphase-separated pore walls. Note that this simple diagram does not reflect the true morphological complexity of microphase-separated diblock copolymers confined within such a hard template. Also note that the pores of the PE template are, in fact, coated with a thin layer of PEP[81] that is not shown for simplicity.

to several parameters: the natural periodicity and segregation state of the polymer in the bulk, the shape, size, and dimensionality of the confining geometry, and the interactions of each block with the surface of the confining template. A frequently used confining template is anodic aluminum oxide (AAO).[50−63] AAO films possess cylindrical pores with highly tunable diameters, oriented with their long axis parallel to the film thickness.[64,65] Block polymers are infiltrated into AAO through capillary action, either from solution or in the melt state. After self-assembly of the block polymer, cylindrical nanorods or nanotubes, having internal mesostructure from the segregation of incompatible blocks, are conveniently obtained by dissolution of the AAO template. The internal mesostructure has been exploited to render such nano-objects mesoporous by selective etching[56] or by selective swelling and collapse[57,59,61,63] of a specific component. Even further, Wang *et al.*[59] and Chen *et al.*[61] have demonstrated that such mesoporous nano-objects are effective templates in the preparation of mesoporous, inorganic nano-object replicas.

Various processing strategies have also been used to define a template for the confinement of block polymers. Coaxial electrospinning has been utilized to produce composite nanofibers with narrow diameter distributions, composed of a thermally robust shell surrounding a block polymer core.[66−72] Subsequent annealing of the nanofibers at temperatures where the core and shell are in melt and solid states, respectively, enables the self-assembly of the block polymer within a cylindrical confinement. Alternatively, block polymers have been precipitated from mixtures of a volatile good solvent and nonvolatile nonsolvent by slow evaporation of the former. The block polymer is effectively confined in three dimensions by the spherical shape of the resultant nanoparticles.[73−75] In a related approach, nanoparticles comprising blends of polystyrene (PS) and poly(methyl methacrylate) (PMMA) homopolymers and a PS-PMMA diblock copolymer have been prepared by slow evaporation of toluene from a continuously stirred dispersion of polymer solution in surfactant-loaded aqueous media.[76,77]

We have used nanoporous polyethylene (PE), derived from a polymeric bicontinuous microemulsion (BμE), as a novel template for the confinement of several different diblock copolymers and diblock copolymer/homopolymer blends. Polymeric BμEs are equilibrium disordered melt phases found universally in ternary blends of two immiscible homopolymers A and B and their corresponding A−B diblock copolymer.[78,79] They consist of interpenetrating networks of A and B with vanishing interfacial tension, near-zero mean interfacial curvature, and periodicity on the order of 100 nm. Previously, we have demonstrated that nanoporous PE can be obtained from a PE/poly(ethylene-*alt*-propylene) (PEP) BμE by crystallization of the former and selective solvent extraction of the latter.[80,81] In addition, we have shown that this nanoporous PE can be used as a hard template in the synthesis of robust, single-phase materials, such as ceramics and thermosets. These materials have three-dimensionally continuous pore networks that replicate the original BμE structure with high precision.[80,81] The pores are of uniform shape and size, centered at ∼100 nm and predictable from scattering of radiation by the original BμE. Very recently, we have further shown that hierarchically structured organic−inorganic composites and hierarchically porous silica—having discrete, bicontinuous pore networks differing in size by over an order of magnitude—are readily obtained by confinement of mesostructured silica within the same PE template.[82]

The simple, general process used to confine and self-assemble diblock copolymers within BμE-derived, nanoporous PE is shown in Figure 1. Three copolymer systems have been studied: poly(styrene-*b*-isoprene) (PS-PI), poly(isoprene-*b*-dimethylsiloxane) (PI-PDMS), and poly(isoprene-*b*-2-vinylpyridine) (PI-P2VP), as well as blends of PI-P2VP with PI or P2VP homopolymer.

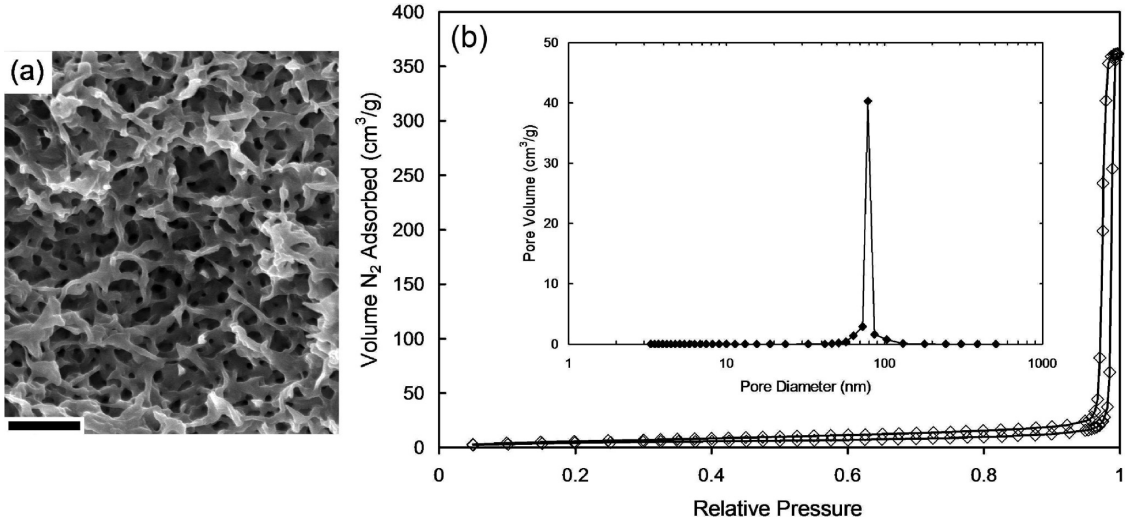

Figure 2. (a) SEM image of the fracture surface of a BμE-derived nanoporous PE monolith used as a template for the confinement of diblock copolymers and diblock copolymer/homopolymer blends. The scale bar indicates 1 μm. (b) Nitrogen sorption data for the same monolith. The main panel shows the adsorption−desorption isotherm, while the inset shows the pore size distribution calculated from the desorption branch by the method of Barrett, Joyner, and Halenda.[89]

After infiltration and self-assembly of the copolymers within nanoporous PE, hierarchically structured materials are obtained, having BμE-like periodicity between PE and copolymer domains, and microphase separation within the latter. The two distinct length scales of structural organization differ by factors ranging from less than two to greater than five. Fleury and Bates have previously reported similar hierarchically structured materials by extension of the thermodynamic principles underlying BμE formation to include more complex, multiblock architectures; however, crystallization of one component was used to induce microphase separation, resulting in ill-defined morphologies.[83] The present confined copolymer morphologies observed are similar to those reported for the confinement of block polymers within AAO and are rationalized in the context of the previous work. However, unlike AAO or any of the above-mentioned examples, the bicontinuous nature of the PE template affords the opportunity to generate hierarchically structured porous materials by postremoval of the template. This is demonstrated with PI-P2VP as a model system, wherein the majority P2VP block is cross-linked and the PE template is removed by selective solvation. A porous monolith is obtained, having a three-dimensionally continuous network of ~100 nm pores, while the microphase separation between PI and P2VP is undisturbed within the pore walls. To the best of our knowledge, the only other materials reported for which porous block polymer monoliths with confined morphologies can be obtained are colloidal crystal templates.[84−87] In contrast to the three-dimensional confinement provided by such templates, the unique structure of BμE-derived, nanoporous PE confers a decidedly two-dimensional character to the confined morphologies, despite the overall three-dimensional connectivity of the copolymer domains. The approach to hierarchically structured, self-supporting polymeric monoliths described herein is anticipated to be applicable to supported thin films[88] and, furthermore, is expected to ultimately be extended to the production of hierarchically porous materials.

RESULTS AND DISCUSSION

Figure 2 summarizes the pore characteristics of the BμE-derived, nanoporous PE monoliths used as a template for the confined self-assembly of block polymers. The scanning electron microscopy (SEM) image shown in Figure 2a indicates that the monoliths possess a three-dimensionally continuous and highly tortuous pore network. Importantly, the pore walls are coated with a thin layer of PEP.[81] In Figure 2b, a nitrogen sorption isotherm is provided. The isotherm clearly exhibits a hysteresis loop with a step increase in the volume of N_2 adsorbed at high relative pressures, indicative of capillary condensation within the pore system of the material. The pore size distribution calculated from this isotherm according to the method of Barrett, Joyner, and Halenda,[89] plotted as dV/d[log r] *versus* 2r, where V and r are the cumulative pore volume and pore radius, respectively, is shown in the inset to Figure 2b. The plot reveals a relatively narrow distribution in pore size with an average diameter (D_{ave}) of 78 nm, calculated as

$$D_{ave} = 2\int_0^\infty \left(\frac{dV}{dr}\right) dr \Big/ \int_0^\infty \frac{1}{r}\left(\frac{dV}{dr}\right) dr$$

The diblock copolymers confined within nanoporous PE are summarized in Table 1. Hereafter, the PI-P2VP copolymers will be referred to as PI-P2VP(6−35) and PI-P2VP(23−11), where the first and second values are the number-average molecular weights, M_n, in kg/mol

of the PI and P2VP blocks, respectively. The PE monoliths were allowed to imbibe tetrahydrofuran (THF) solutions of all four diblock copolymers, after which the solvent was slowly removed over a period of at least one week. The monoliths were immersed in the copolymer solution throughout the drying process, so as to maximize the loading of copolymer within the pores; typical filling values were 60−70% by volume. To determine the bulk morphology of the copolymer under these conditions, excess material surrounding the immersed PE monolith, after drying, was analyzed by a combination of small-angle X-ray scattering (SAXS) and transmission electron microscopy (TEM). In all cases, the resultant data indicated that this slow solvent removal procedure was sufficient to access the equilibrium bulk morphology, namely, hexagonally packed cylinders. As a representative example, the SAXS pattern and a TEM image of excess, bulk PI-P2VP(6−35) are shown in the Supporting Information (Figure S1), indicating clearly the hexagonal packing of PI cylinders in a P2VP matrix.

TABLE 1. Diblock Copolymers and Homopolymers Used in Preparation of Hierarchically Structured Materials

polymer	M_n (kg/mol)[a]	M_w/M_n[b]	f_{PI}[c]
PS-PI	92	1.08	0.75
PI-PDMS	30	1.06	0.76
PI-P2VP	41	1.10	0.18
PI-P2VP	33	1.01	0.73
PI	3.8	1.05	1
P2VP	9.5	1.16	0

[a] Number-average molecular weight determined by size exclusion chromatography (SEC). [b] Polydispersity index determined by SEC; M_w is the weight-average molecular weight. [c] Volume fraction of PI at room temperature determined from nuclear magnetic resonance (NMR) spectroscopy, calculated using densities of 0.900, 1.049, 0.970, and 1.145 g/cm^3 for PI, PS, PDMS, and P2VP, respectively.[90−92]

In Figure 3 and Figure 4, TEM images of the hierarchically structured materials obtained by confinement of PI-P2VP(6−35) and PS-PI, respectively, within nanoporous PE are provided. The corresponding images for PI-PDMS are of significantly poorer quality and are reserved for the Supporting Information (Figure S2). For both PI-P2VP(6−35) and PS-PI, the TEM images reveal the distinct hierarchical arrangement of matter in these materials. In the low-magnification

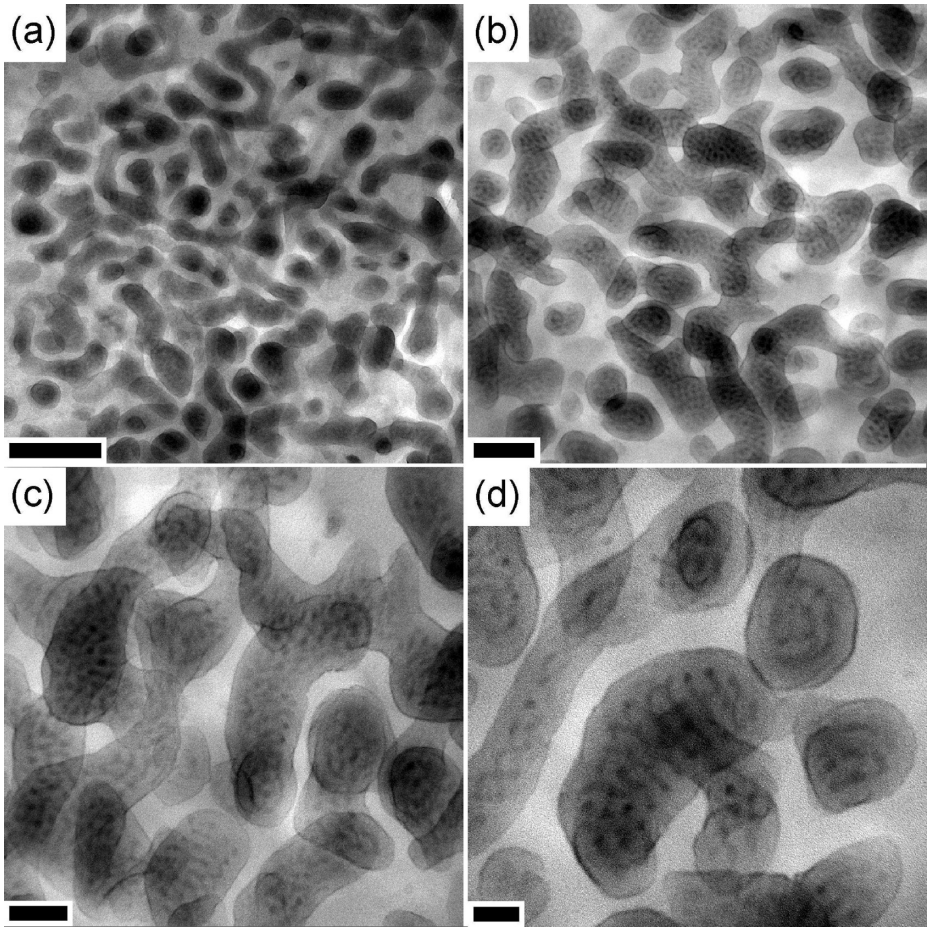

Figure 3. TEM images of hierarchically structured material obtained from infiltration of PI-P2VP(6−35) into nanoporous PE. The magnification increases monotonically from panel a through panel d. After infiltration, the material was exposed to the vapor of diiodobutane to cross-link the P2VP block of the copolymer. The material was further stained with OsO_4. The PE, P2VP, and PI domains appear bright, medium, and dark, respectively. Scale bars indicate (a) 400 nm, (b) 200 nm, (c) 100 nm, and (d) 50 nm.

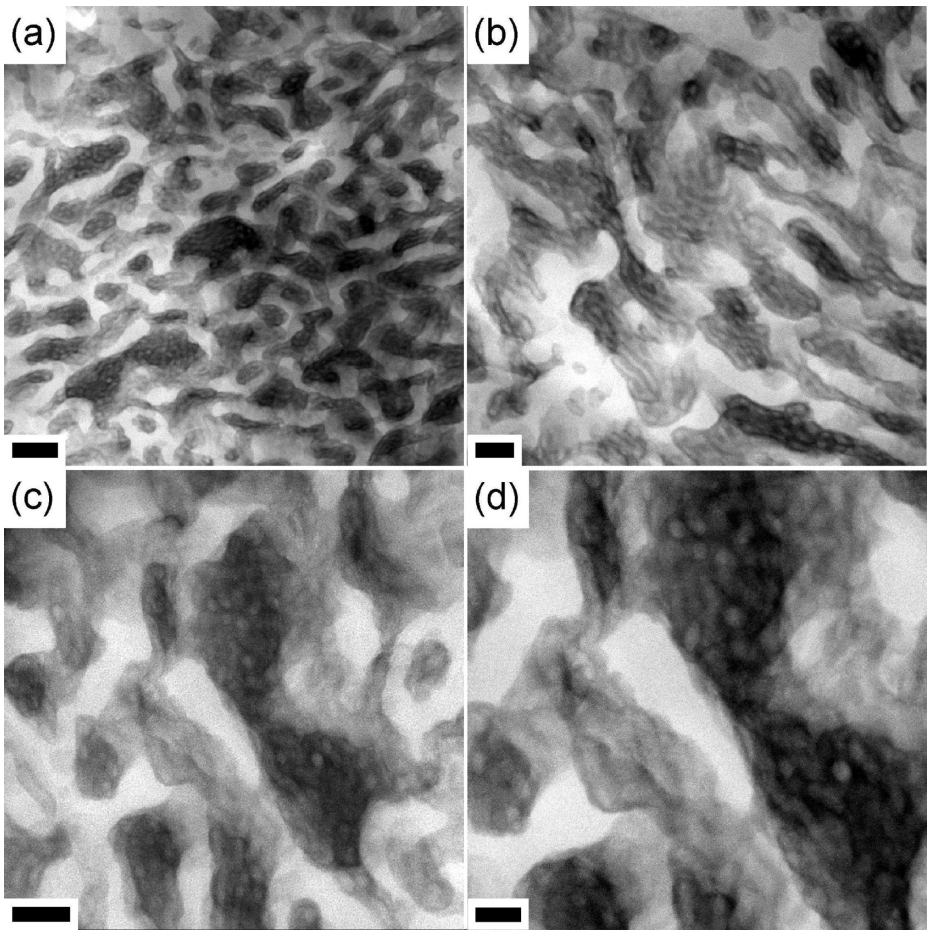

Figure 4. TEM images of hierarchically structured material obtained from infiltration of PS-PI into nanoporous PE. The magnification increases monotonically from (a) through (d). The material is stained with OsO_4, a preferential stain for PI. The PE and PS appear bright, while the PI appears dark. Scale bars indicate (a) 200 nm, (b,c) 100 nm, and (d) 50 nm.

views (parts a and b of Figure 3 and Figure 4), the BμE structure provided by the PE template is apparent, with discrete, interpenetrating networks of PE and copolymer appearing bright and dark, respectively. Closer examination of the latter (parts c and d of Figure 3 and Figure 4) reveals a remarkably complex arrangement of microphase-separated domains within the confined copolymer network. The two levels of structural organization differ in the length scales of their periodicity by over a factor of 5 and 3 for PI-P2VP(6−35) and PS-PI, respectively. In both cases, the PI appears darker than the P2VP or PS, due to the higher electron density conferred by an OsO_4 stain of PI. For PS-PI, the PS and PE appear equally bright, whereas for PI-P2VP, the P2VP is significantly darker than PE, due to the enhancement of electron density from the cross-linking of P2VP by diiodobutane. Thus, the images in Figure 4 have only a single level of contrast, whereas the images in Figure 3 have three distinct levels of contrast.

For the PE/PI-P2VP(6−35) material (Figure 3c,d), as the copolymer network is traversed from the PE−copolymer interface to the core of the copolymer domain, three distinct regions of segregation are clearly observed, critically enabled by the multiple levels of contrast. First, a thin layer of PI resides at the PE−copolymer interface, having a thickness of several nanometers. This wetting layer signifies the preference of PI over P2VP to form an interface with the PEP coating the pore walls of the PE template. Indeed, this can be rationalized from a purely enthalpic standpoint, as PI and PEP are composed of hydrophobic, nonpolar repeat units, while P2VP is substantially more polar. The value of χ between PEP and PI, $\chi_{PEP\text{-}PI}$, is almost 14 times smaller than $\chi_{PI\text{-}P2VP}$;[93,94] from this, it can reasonably be inferred that $\chi_{PEP\text{-}PI} < \chi_{PEP\text{-}P2VP}$, which supports the observed wetting phenomenon. Second, adjacent to this PI wetting layer, there is a significantly thicker layer that appears to be rich in P2VP. Presumably, the formation of the PI layer at the PE−copolymer interface depletes the near-interface region of that component. As PI only constitutes 18 vol % of PI-P2VP(6−35), the near-interface region consequently must be composed of an overwhelming fraction of P2VP. Similar phenomena have been observed in diblock copolymer thin films which exhibit preferential wetting of one block to a substrate.[95] Third, toward the interior of the copolymer regions, a variety of PI objects

dispersed in a continuous matrix of P2VP are observed. In many cases, it is difficult to discern the exact shape and connectivity of the dispersed PI domains because of the overlapping of randomly oriented, adjacent domains caused by the projection of the three-dimensional sample volume into a two-dimensional image. Objects having cylinder-, disk-, and helix-like shapes are all apparent. For example, toward the left side of Figure 3d, a double helix of PI appears to run through the core of the copolymer domain, with the long axis of the helix parallel to the PE−copolymer interface. In other instances, small clusters of hexagonally packed cylinders can be distinguished. From the SAXS pattern of PI-P2VP(6−35) (Figure S1), the bulk equilibrium period (*i.e.*, the cylinder−cylinder spacing) and the cylinder diameter of PI-P2VP(6−35) are 31.2 ± 0.7 and 13.4 ± 0.3 nm, respectively. In general, the PI objects in Figure 3c,d appear to have spacings and diameters similar to these values.

On the other hand, the single level of contrast in Figure 4 precludes full elucidation of the microphase-separated structure of confined PS-PI. Specifically, it cannot be conclusively discerned from the TEM images whether the PS or PI block (or neither) preferentially wets the pore walls of the template. $\chi_{PEP\text{-}PS}$ is nearly 5 times greater than $\chi_{PEP\text{-}PI}$,[93] suggesting that PI is also the preferred wetting component in this system; however, as discussed later, the packing frustration induced by confinement of the copolymer can potentially overwhelm wetting tendencies in the determination of overall morphology. Nevertheless, the microphase-separated morphology of the confined PS-PI appears similar to that of PI-P2VP(6−35), except that PI now comprises the majority component of the copolymer. Short cylinder- and disk-like objects, and potentially spherical objects, comprising PS are dispersed within a continuous matrix of PI. Unlike PI-P2VP(6−35), no extended helix structures were observed and there is no clear evidence of hexagonal ordering within larger pores. The bulk equilibrium period and cylinder diameter of PS-PI determined by SAXS are 48.1 ± 0.9 and 19.8 ± 0.4 nm, respectively. As before, the dispersed PS objects in Figure 4c,d appear to have spacings and diameters similar to these values.

As mentioned previously, the self-assembly behavior of confined block polymers has been studied by other researchers in detail.[49] Much of this work has focused on the behavior of diblock copolymers confined within cylindrical geometries, such as AAO films or coaxially electrospun nanofibers.[50−63,66−72] Under such confinement, copolymers were indeed found to exhibit morphologies significantly rearranged relative to the bulk equilibrium state. The particular confined state results from a balance of the natural periodicity of microphase separation, the frustration induced by confinement, and the interactions of each block with the confining pore walls. Naturally, the morphology depends critically on the ratio of the confining pore diameter (D) to the bulk equilibrium period of the copolymer (L_0). For example, poly(styrene-*b*-butadiene) (PS-PB), forming cylinders of PB in a continuous PS matrix in the bulk, was found to exhibit PB disks and torus-like structures stacked vertically along the long axis of AAO pores at D/L_0 ratios of 0.92 and 1.0, respectively.[58] Single and double helices of PB running parallel to the AAO pore axes were discovered at D/L_0 ratios of 1.27 and 1.6, respectively. Combinations of PB rings, single cylinders, and helices, and even a triple helix, were observed for $1.81 < D/L_0 < 2.22$. Finally, for $D/L_0 > 2.3$, the copolymer adopted the bulk morphology; that is, hexagonally packed cylinders of PB were observed. When the same copolymers were infiltrated into carbon nanotubes, equivalent confined morphologies were obtained, although they were shifted to lower values of D/L_0. This was assumed to be a consequence of different interaction energies between the copolymer blocks and the pore walls. In some cases, the entropic penalty of the copolymer frustration induced by confinement was sufficient to overwhelm the tendency of PB to wet the pore wall−copolymer interface; that is, the normally nonwetting PS block was found at the interface.

The copolymer morphologies observed presently in hierarchically structured PE/PS-PI and, in particular, PE/PI-P2VP(6−35) are consistent with these previous investigations. The pore network presented by the PE template can be considered as a series of tortuous pathways with cylindrical or near-cylindrical cross sections. The tendency for dispersed domains to align parallel to the pore walls, as in AAO, is apparent from Figure 3 and Figure 4. Apparently, for PI-P2VP(6−35) in PE, any entropic penalty imposed by the copolymer frustration from confinement is insufficient to overwhelm the wetting tendency exhibited by the system since PI is exclusively observed at the copolymer-PE interface. This is reasonable, given the extreme enthalpic penalty associated with the formation of a P2VP wetting layer compared to a PI one, as discussed previously. The confining pore diameters span roughly 60−100 nm; this range accounts for ∼95% of the total pore volume seen in the pore size distribution of Figure 2b. The corresponding D/L_0 values for PI-P2VP(6−35) should thus range from 1.9 to 3.2. Therefore, on the basis of previously reported work, the confined PI-P2VP(6−35) should be anticipated to exhibit a range of morphologies. In fact, the total thickness of the PI wetting and P2VP-rich depletion layers surrounding the core of the copolymer regions appears to be significantly thicker than the corresponding layers in AAO/PS-PB composites.[51] This suggests that the space into which these unique microphase-separated morphologies are assembled is effectively smaller, relative to the pore diameter, in the present system. Indeed, the D/L_0 ratio for the pore containing the PI double

helix on the left side of Figure 3d is estimated to be 2.3, yet an equivalent structure was observed in AAO/PS-PB composites at a D/L_0 ratio of only 1.6.[58] In other words, these observations lend further support to the notion that confined copolymer morphologies are critically linked not only to D/L_0 but also the copolymer composition and the difference in interactions between the respective blocks and the pore walls. Similarly, the D/L_0 values for PS-PI in pores of diameter spanning 60−100 nm should range from 1.2 to 2.1. The PS-PI should thus also be expected to self-assemble into a variety of morphologies. The larger equilibrium bulk period of PS-PI, relative to PI-P2VP(6−35), suggests that the former would display morphologies more characteristic of a greater degree of confinement, that is, disk-like, torus-like, and single- and double-helix structures. This may be counterbalanced, though, to some extent by the lessened propensity of PI to wet the PE−copolymer interface, as well as the fact that PI is the majority component. The exact reason as to why no extended helical structures were clearly observed in PE/PS-PI composites by TEM (Figure 4) is unclear; however, the lack of contrast between PE and PS, coupled with the complex three-dimensional structure of the overall material, undoubtedly complicates determination of the local morphologies observed in these images.

On the opposite end of the spectrum, the TEM images in Figure 3 and the estimated D/L_0 ratios suggest that some fraction of PI-P2VP(6−35) within the largest pores of the PE template is arranged in its bulk morphology, that is, hexagonally packed cylinders of PI, having the long axis of the cylinders oriented parallel to the pore walls. This is further supported by the SAXS pattern of the PE/PI-P2VP(6−35) composite, presented in Figure 5. For comparison, the pattern of bulk, cross-linked PI-P2VP(6−35) is also provided. The pattern of the hierarchically structured composite material displays the characteristic signs of both levels of structural organization. Significant scattering is present at low values of q due to the BμE structure imposed by the PE template. A broad peak following the form of the Teubner−Strey model[96] is expected, although it is cut off at low q by the beam stop. This, in fact, mimics the scattering behavior of the original BμE from which the nanoporous PE template was derived.[81] At higher q, two shoulders are noticeable in the pattern. By comparison with the pattern directly below, it appears that these shoulders are broadly consistent with the microphase separation of the copolymer. The relatively poor definition of these shoulders involves several factors. The microemulsion peak still contributes significantly to the overall scattering of the material at higher q and, thus, may obscure the scattering contribution of the PI-P2VP. Furthermore, the PI-P2VP only constitutes less than half of the material volume sampled by the incident X-ray beam. Of this portion, the TEM images in Figure 3 unquestionably show that much of the PI-P2VP does not adopt the bulk, hexagonal packing, as discussed. Even still, those regions of hexagonal ordering which give rise to the diffraction shoulders in Figure 5 are limited in the extent of their long-range correlation by the confining geometry. Essentially, the effective grain sizes of any ordered domains are necessarily small, implying significant broadening of the corresponding Bragg diffraction features.

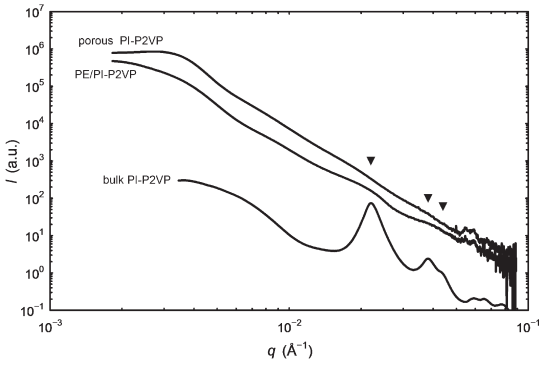

Figure 5. SAXS patterns, from bottom to top, of bulk PI-P2VP (6−35) after diiodobutane cross-linking; hierarchically structured PE/PI-P2VP(6−35) composite after diiodobutane cross-linking; and porous PI-P2VP material generated by selective solvent extraction of PE template from PE/PI-P2VP(6−35) composite. The patterns have been shifted vertically for clarity. The three markers, from left to right, denote the first three reflections of hexagonal symmetry: q^*, $3^{1/2}q^*$, and $4^{1/2}q^*$, where q^* is the value corresponding to the principal peak of bulk PI-P2VP(6−35).

Using PI-P2VP as a model system, we have also conducted a preliminary investigation into the morphologies exhibited as the relative composition of confined material is varied. To increase the overall fraction of PI while maintaining a majority fraction of P2VP, blends containing PI-P2VP(6−35) and PI homopolymer (Table 1) were infiltrated into nanoporous PE. In addition, PI-P2VP(23−11), which forms hexagonally packed cylinders of P2VP in a continuous PI matrix in the bulk, and its blends with P2VP homopolymer (Table 1) were used to achieve a majority fraction of PI. Representative TEM images of the various hierarchically structured materials that were observed are provided in Figure 6. Low-magnification views are not provided, as they show essentially the same BμE-like arrangement of PE and PI-P2VP seen, for example, in Figure 3a,b. Figure 6a,b shows the confined morphology of a PI-P2VP(6−35)/PI blend containing 40 vol % PI. This blend still exhibits a cylinder-type morphology, akin to that of pure PI-P2VP(6−35), but the larger natural period induced by swelling of PI domains with homopolymer is readily apparent. At the entire interface between the blend and the PE template, PI wetting and adjacent P2VP-rich layers are again observed. For smaller pore sizes, however, the interior regions of the copolymer domains are composed entirely of PI.

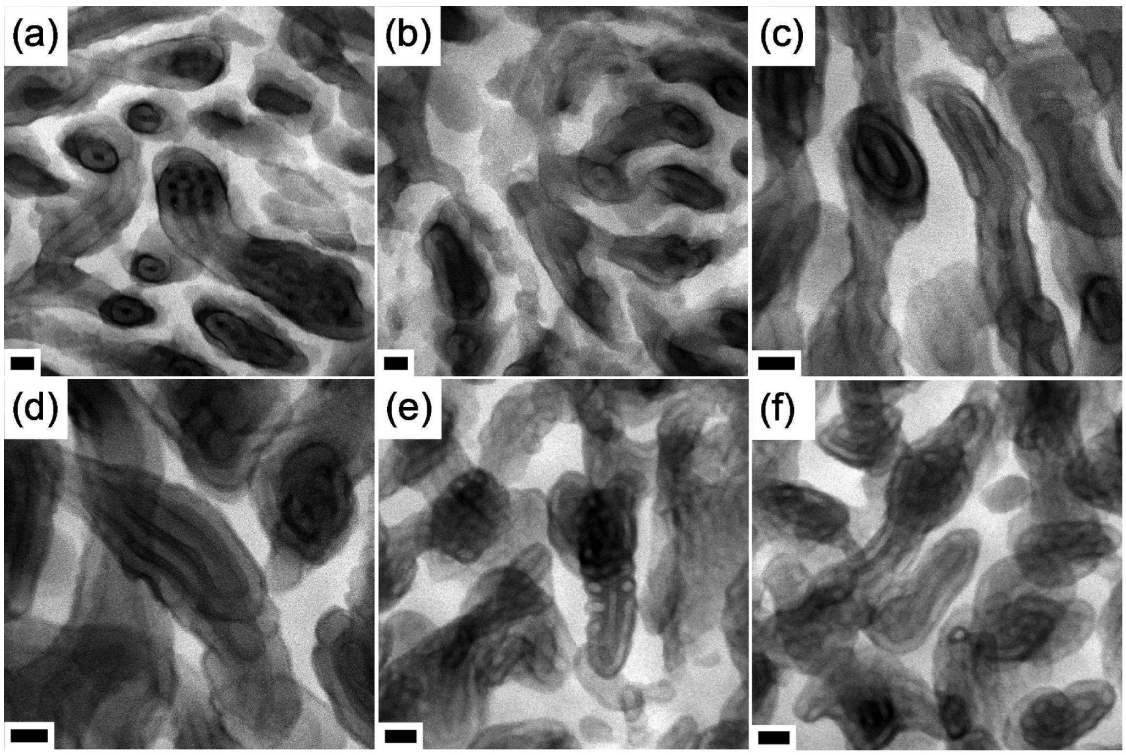

Figure 6. TEM images of hierarchically structured materials obtained from infiltration of (a,b) PI-P2VP(6−35)/PI blend with f_{PI} = 0.40; (c,d) PI-P2VP(23−11)/P2VP blend with f_{PI} = 0.61; and (e,f) PI-P2VP(23−11)/P2VP blend with f_{PI} = 0.71 into nanoporous PE. After infiltration, all materials were exposed to the vapor of diiodobutane to cross-link the P2VP component of the blends. The materials were further stained with OsO_4. The PE, P2VP, and PI domains appear bright, medium, and dark, respectively. Scale bars indicate 50 nm.

This results in a PI/P2VP/PI core/shell/shell-type structure, aligned along the confining pore walls. The cross-sectional view of this structure, as in several locations in Figure 6a,b, appears as a circular or oblong PI domain surrounded by successive thick P2VP and thin PI annuli. Even further, Figure 6b provides insight into the manner in which the PI and P2VP assemble to accommodate the complex confining geometry occurring at the local intersection of adjacent PE pores, a Y-shaped junction can clearly be seen, wherein a single core/shell/shell motif splits into two equivalent structures. For larger pores, multiple cylindrical PI domains are aligned parallel to the pore walls, separated by a continuous P2VP matrix. A representative example is seen in Figure 6a, spanning from the center to the lower-right corner of the image.

Further increases in PI content of the infiltrated material enables access to morphologies characteristic of confined, lamellae-forming copolymers. Figure 6c,d shows the confined morphology of a PI-P2VP(23−11)/P2VP blend containing 61 vol % PI. In this case, both the PI and P2VP form alternating layered structures. Again, a PI wetting layer is exclusively enforced across the entire PE−blend interface. Where the confining pore channels are oriented perpendicular to the image plane, the cross section of the copolymer domains is visible and consists of concentric, alternating annuli of PI and P2VP. At first glance, the morphology of this particular blend may appear qualitatively identical to that of the blend containing 40 vol % PI (Figure 6a,b). However, note that in the largest pores observed, the 40% blend clearly arranges into cylindrical entities of PI, whereas the 61% blend solely exhibits layered structures; that is, there is no clear continuous or dispersed component. Indeed, similar morphologies have been observed for symmetric PS-PB copolymers confined within AAO.[51,58] When the PI content is increased yet further, morphologies characteristic of confined, cylinder-forming copolymers are again obtained, instead consisting of P2VP objects dispersed in a continuous matrix of PI. Figure 6e,f shows the confined morphology of a PI-P2VP(23−11)/P2VP blend containing 71 vol % PI. The detailed internal arrangement of the PI and P2VP domains is not quite the inverse of that seen with pure PI-P2VP(6−35) (Figure 3c,d). The interface between the copolymer and the PE template, at present, is still exclusively wetted by PI. However, there is no P2VP-rich layer immediately adjacent to this PI wetting layer, unlike the confined PI-P2VP(6−35). The depletion of P2VP at the interface apparently does not necessitate the segregation of P2VP to the near-interface region because of the comparatively small fraction of P2VP in the blend. Apart from this consideration, the interior of the copolymer domains exhibits a similar, microphase-separated morphology to that seen with

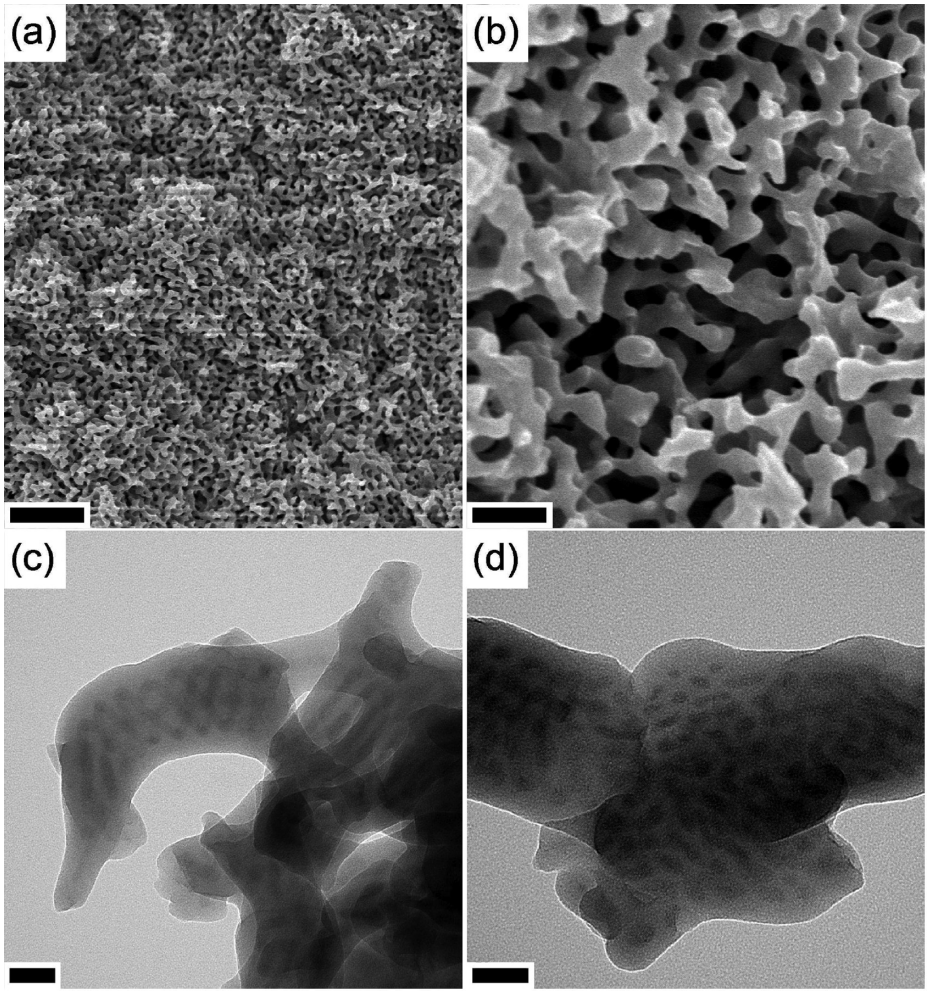

Figure 7. (a,b) SEM images of porous PI-P2VP material resulting from selective extraction of PE from hierarchically structured PE/PI-P2VP(6−35) composite with heptane at 85 °C. Scale bars indicate (a) 1.5 μm and (b) 300 nm. (c,d) TEM images of the same material. The sample was ground into a fine powder and dispersed on a grid for analysis; the images show small fragments generated from the destruction of the porous framework. The powder was further stained with OsO_4 vapor to render the PI domains dark. Scale bars indicate 50 nm.

PI-P2VP(6−35). Specifically, cylinders, disks, and helices, in this case composed of P2VP, are dispersed in a continuous matrix of PI and oriented parallel to the PE walls.

The hierarchically structured PE/PI-P2VP composites characterized above were further utilized as precursors to porous materials through selective extraction of the PE template. We present here representative results obtained with the PE/PI-P2VP(6−35) composite shown in Figure 3. Two different good solvents for PE were employed in separate experiments. After soaking in toluene at 72 °C, the fracture surface of the resultant porous material (Supporting Information, Figure S3) does not possess the characteristic pore structure of BμE-templated materials. Hot toluene is actually a good solvent for PE, PI, and P2VP, while diiodobutane cross-linked PI-P2VP films, separately immersed in toluene, showed a tendency to disintegrate, although not dissolve. Besides selectively extracting the PE template, the toluene solvent apparently swells the PI-P2VP domains of the composite to such a degree that a bicontinuous pore structure cannot be supported. In contrast, the use of heptane at 85 °C—a good solvent for PE and PI but a poor solvent for P2VP—selectively extracts the PE template but does not significantly affect the PI-P2VP domains. The SEM images provided in Figure 7a,b demonstrate that the BμE structure is imprinted into a porous PI-P2VP monolith over large areas. The pores possess sizes on the order of 100 nm and are clearly interconnected in three dimensions. The latter property results from the bicontinuous structure of the PE template,[80,81] which is further proven by the monolithic nature of the porous PI-P2VP. The SAXS pattern of this material, shown in Figure 5, exhibits the same features as its composite precursor, namely, scattering indicative of both the large scale BμE pore structure and the microphase separation of the PI-P2VP within the pore walls. The TEM images provided in Figure 7c,d further demonstrate that the unique morphology of the confined PI-P2VP is retained after exposure to hot heptane. In the

central portion of Figure 7c, for example, a double helix surrounding a single cylinder of PI can clearly be discerned. Quite remarkably, the BμE pore structure can also be observed, to a certain extent, after the heptane extraction of PE from the PE/blend composite where the blend comprises 71 vol % PI (Figure 6e,f). SEM images provided in the Supporting Information (Figure S4) demonstrate substantial pore collapse in this case, but the signature of the BμE structure is still evident. We did not expect this result, given the majority fraction of PI—a liquid at room temperature—in the blend. Apparently, the connectivity of the P2VP objects dispersed within the copolymer network confers substantial mechanical stability to the overall material.

These complex porous materials represent an unprecedented example of the design of hierarchical nanostructure by block polymer confinement. As mentioned previously, the only previously reported strategies in which confined block polymers are released from their templates as monolithic porous materials utilize colloidal crystals.[84−87] In contrast to these examples, the nanoporous PE template imparts a confining geometry that enables access to two-dimensionally confined morphologies, such as helical structures, yet the overall block polymer is interconnected in three dimensions. We anticipate that the PI-P2VP model system which we have utilized can be further extended as a precursor to hierarchically porous materials. To date, there have been few reported examples of hierarchically porous polymeric materials; of these reports, at least one of the pore structures is generally of ill-defined shape, size, or connectivity.[36,97−100] We have begun preliminary experiments to selectively void the PI microdomains of our porous PI-P2VP materials by chemical etching. The resulting materials are expected to have complex hierarchical arrangements of uniformly sized mesopores and macropores, replicated from the block polymer confined morphology and BμE-derived template, respectively. The pore structures that are envisioned by this route should confer both high surface area and low mass transport barriers to the resultant materials. These characteristics, coupled with the unique properties of P2VP, for example, its ability to complex and hydrogen bond, will enable the rational design of advanced, functional materials for applications in catalysis and sensors, among others.

CONCLUSIONS

BμE-derived nanoporous PE has been used as a template in the creation of several novel hierarchically structured materials by the confined self-assembly of diblock copolymers and diblock copolymer/homopolymer blends. The product materials exhibited a BμE-like arrangement of discrete PE and copolymer (or blend) networks; within the latter, an additional microphase-separated arrangement of matter was clearly present. A rich variety of microphase-separated structures were observed, including cylinder-, disk-, and helix-like objects of one component dispersed in a continuous matrix of the other, as well as annular, alternating layers, depending on the composition of the confined material. These morphologies were consistent with previous literature regarding the confinement of diblock copolymers and could be justified by considering a balance of interfacial phenomena, the natural bulk ordering of the copolymer, and frustration induced by confinement. Using the model system of PI and P2VP, well-defined porous materials were successfully prepared by cross-linking of the P2VP and selective extraction of the PE template. The materials contained a three-dimensionally continuous ~100 nm pore network having P2VP pore walls within which ~10 nm diameter PI objects were dispersed. These porous materials, while unique in their own right, are further anticipated to be useful precursors to hierarchically porous P2VP, having uniformly sized and complex interconnected networks of macropores and mesopores. These results provide further evidence that BμE-derived nanoporous materials are promising templates in the rational design of porous functional materials.

EXPERIMENTAL METHODS

PS-PI, PI-PDMS, and PI-P2VP diblock copolymers employed in this work were synthesized by anionic polymerization. The molecular characteristics of the copolymers are summarized in Table 1. In all cases, the PI blocks exhibited predominantly 1,4-regioisomers (>90%). PS-PI was synthesized as described previously.[101] PI-PDMS was also synthesized as described previously and purified of PDMS homopolymer impurity as detailed in the same references.[102,103] The two PI-P2VP diblock copolymers were synthesized as follows (all reagents employed were obtained from Aldrich). First, isoprene, previously deoxygenated and purified by two successive vacuum distillations from *n*-butyllithium (supplied as a 2.5 M solution in hexanes), was anionically polymerized at 40 °C using cyclohexane (CHX) as solvent and *sec*-butyllithium (supplied as a 1.4 M solution in CHX) as initiator. The CHX solvent was previously purified by passage over packed alumina and copper oxide on alumina columns. THF was rigorously purified by a two step procedure: first, by passage over packed alumina columns and, second, by vacuum distillation from *n*-butylmagnesium chloride. The CHX solution of living polyisoprenyl anions, having a faint yellow color, was diluted with THF at a ~2:1 volume ratio of THF/CHX, yielding a vivid golden solution. This solution was subsequently cooled to −78 °C, and 2-vinylpyridine, previously purified by successive vacuum distillations from calcium hydride and triethylaluminum, was slowly added. The solution immediately turned a deep red color, and the 2-vinylpyridine was allowed to react at −78 °C for at least 1 h. The reactor was warmed to −50 °C, and the living copolymer chains were terminated with degassed methanol. The solution of PI-P2VP was dried in a rotary evaporator, and the polymer was redissolved in dichloromethane to form a ~8 wt % solution. This solution was slowly

added to ~2 L of hexanes under stirring. For PI-P2VP(6−35), the resulting mixture was cloudy, but the polymer remained suspended when allowed to stand. For PI-P2VP(23−11), the equivalent mixture was a hazy solution. Methanol was added dropwise to these mixtures under stirring until the polymer appeared to be maximally precipitated. After allowing the mixture to stand, PI-P2VP(6−35) had settled to the bottom of the container, allowing the supernatant to be decanted and the polymer to be recovered and dried. In contrast, the mixture containing PI-P2VP(23−11) separated into four distinct layers: a gel, a slightly cloudy liquid, an extremely cloudy liquid, and a clear liquid, from top to bottom. The top three layers were collected and dried and PI-P2VP(23−11) was obtained in 95% yield.

The PI-P2VP copolymers were used in their pure form and also as blends with the homopolymers listed in Table 1. PI homopolymer, possessing the same regiochemistry as the PI blocks of the copolymers (*i.e.*, predominantly 1,4-addition), was synthesized by anionic polymerization using equivalent techniques to those described above. P2VP homopolymer was purchased from Aldrich.

The molecular weight and compositional characteristics listed in Table 1 were determined by SEC and NMR spectroscopy, respectively. SEC measurements were performed in tetrahydrofuran (THF) with Phenomenex Phenogel columns packed with porous beads of 5×10^3, 5×10^4, and 5×10^5 Å pore sizes. The column eluate was analyzed successively by a Wyatt Technology Dawn DSP multiangle laser photometer with a 633 nm helium−neon laser and a Wyatt Technology Optilab DSP interferometric refractometer. The combined light-scattered intensity and refractive index data were analyzed using ASTRA software. Specific refractive index increment values of 0.124, 0.192, 0.005, and 0.155 mL/g were used for PI, PS, PDMS, and P2VP, respectively.[104,105] The total refractive index increment values of the diblock copolymers were calculated by averaging the values of the respective blocks on a mass basis.[106] Proton NMR spectra were acquired using deuterated chloroform as a solvent with a Varian UNITY 300 MHz spectrometer operated at room temperature. Typically, 128 scans were performed and delay and acquisition times of 20 and 3 s were employed, respectively.

Nanoporous PE monoliths were derived from polyolefin BμEs, composed of PE (M_n = 23 kg/mol, M_w/M_n = 1.05), PEP (M_n = 23 kg/mol, M_w/M_n = 1.02), and poly(ethylene-*b*-ethylene-*alt*-propylene) (PE-PEP, M_n = 101 kg/mol, M_w/M_n = 1.07), as described previously.[80,81] Briefly, PE, PEP, and PE-PEP were blended at volume fractions of 0.425, 0.425, and 0.15, respectively, by dissolution in benzene at 70 °C, followed by freeze-drying. The blend was heated to 132 °C and held for 2 h to allow the development of a BμE morphology, after which the PE domains were crystallized by quenching in liquid nitrogen. Finally, nanoporous PE was obtained by selective extraction of the PEP homopolymer with THF.

As-synthesized diblock copolymers and blends were infiltrated into nanoporous PE to create hierarchically structured composites. The diblock copolymer or diblock copolymer and homopolymer were dissolved in THF, typically at 10 wt %. A PE monolith was added to the solution and allowed to rest for at least 1 h. Then, the THF was slowly removed under ambient conditions over the course of 1−2 weeks. This slow removal was intended to maximize the degree of pore filling. An ordered diblock copolymer melt can be directly infiltrated into a porous material (*i.e.*, without solvent);[51] however, the glass transition temperatures, T_g, of P2VP and PS are comparable to the crystalline melting temperature, T_m, of PE, thus prohibiting the infiltration of copolymers or blends containing such components as pure melts. Due to the same restrictions, the equilibrium copolymer morphologies could not be achieved by annealing in the melt state. Therefore, slow solvent removal is also necessary to avoid the existence of kinetically trapped, non-equilibrium morphologies. The PE monolith, having diblock copolymer confined within its pores, was removed and excess copolymer coating the external surfaces was removed.

After infiltration, PE/PI-P2VP composites were exposed to diiodobutane vapor to cross-link the P2VP chains. Iodine species quaternize the nitrogen atom in the pyridine ring of P2VP, thus forming butyl bridges between P2VP repeat units. A large excess of diiodobutane liquid was placed in a flask, along with a vial containing the PE/PI-P2VP monolith. The flask was sealed and subjected to freeze−pump−thaw cycles to remove oxygen. Finally, the flask was immersed in an oil bath heated to 80 °C for 48 h. Previous research suggests that this procedure should result in quaternization of nearly all P2VP units.[107,108] However, weight measurements before and after cross-linking indicated that only ~30−50% of the P2VP units had reacted, assuming that each diiodobutane molecule quaternized two P2VP units. Increasing the duration of the reaction caused negligible increases in cross-linking extent. In addition, similar results were obtained in the cross-linking of pure copolymer. Nevertheless, the cross-linked copolymer was intractable in solvents like THF—a good solvent for both PI and P2VP—indicating substantial interchain cross-linking. The cross-linked PE/PI-P2VP composites were then soaked in toluene at 72 °C or heptane at 85 °C to selectively extract and void the PE domains and subsequently dried under vacuum.

TEM was performed to investigate the morphologies exhibited by the various hierarchically structured materials. A FEI Tecnai G^2 F30 field emission gun instrument was used, operated at 300 kV accelerating voltage. Images were obtained with an Ultrascan 4000 by 4000 pixel charge-coupled device camera. The analyzed samples consisted of two different forms. Hierarchically structured composite materials, still containing the PE template, were cut into ~85−200 nm sections at −150 to −80 °C using a Leica UC6 cryogenic ultramicrotome. These sections were then dispersed onto an uncoated copper mesh grid. Porous materials obtained after the removal of PE, being significantly more brittle in general, were ground into a fine powder with a ceramic mortar and pestle. This powder was then dispersed onto a carbon-coated copper mesh grid. SEM was used to analyze the pore structures of the nanoporous PE template and the porous PI-P2VP materials obtained by selective dissolution of the template. A Hitachi S-900 microscope was used at operating voltages ranging from 2 to 5 kV. Fracture surfaces were created in liquid nitrogen by breaking samples with tweezers. These fracture surfaces were mounted on metal stubs *via* conductive carbon tape and coated with ~2 nm of Pt using a VCR indirect ion-beam sputtering system. SAXS experiments were conducted using synchrotron radiation generated at the Argonne National Laboratories Advanced Photon Source using the Sector 5-ID-D beamline maintained by the Dow−Northwestern−DuPont Collaborative Access Team. Samples were adhered to plastic washers using Kapton tape. X-rays with wavelengths of either 0.73 or 1.38 Å and a sample-to-detector distance of 6.12 m were used. The X-rays scattered by the samples were collected using a two-dimensional area detector. The obtained two-dimensional scattering patterns were exclusively isotropic and were azimuthally integrated to obtain one-dimensional plots of scattered intensity *I versus* wavevector *q*. Finally, nitrogen sorption measurements were conducted at 77 K using a Quantachrome Instruments Autosorb iQ. Samples were degassed at room temperature for 6 h prior to measurement.

Acknowledgment. This work was supported by the MRSEC program of the National Science Foundation under Award No. DMR-0819885. B.H.J. was also supported partially by a University of Minnesota Doctoral Dissertation Fellowship. Portions of this work were carried out using instrumentation provided by the University of Minnesota Characterization Facility. We gratefully acknowledge Dr. Soo-Hyung Choi, Brian Habersberger, and Prof. Kevin Cavicchi for synthesizing and providing the PS-PI, PI homopolymer, and PI-PDMS, respectively. We also acknowledge Yu Lei, Chris Frethem, and Dr. Wei Zhang for helpful discussion.

Supporting Information Available: SAXS pattern and TEM image of bulk PI-P2VP(6−35); TEM images of hierarchically structured PE/PI-PDMS composite; SEM images of porous materials obtained by selective toluene extraction of PE from PE/PI-P2VP-(6−35) composite and heptane extraction of PE from PE/PI-P2VP/P2VP composite with blend having 71 vol % PI. This material is available free of charge *via* the Internet at http://pubs.acs.org.

REFERENCES AND NOTES

1. Wei, W.; Yang, Z. Template Synthesis of Hierarchically Structured Composites. *Adv. Mater.* **2008**, *20*, 2965–2969.
2. Hu, J.-S.; Zhong, L.-S.; Song, W.-G.; Wan, L.-J. Synthesis of Hierarchically Structured Metal Oxides and Their Application in Heavy Metal Ion Removal. *Adv. Mater.* **2008**, *20*, 2977–2982.
3. Tokarev, I.; Minko, S. Multiresponsive, Hierarchically Structured Membranes: New, Challenging, Biomimetic Materials for Biosensors, Controlled Release, Biochemical Gates, and Nanoreactors. *Adv. Mater.* **2009**, *21*, 241–247.
4. Yang, X.-Y.; Li, Y.; Lemaire, A.; Yu, J.-G.; Su, B.-L. Hierarchically Structured Functional Materials: Synthesis Strategies for Multimodal Porous Networks. *Pure Appl. Chem.* **2009**, *81*, 2265–2307.
5. Barthlott, W.; Neinhuis, C. Purity of the Sacred Lotus, or Escape from Contamination in Biological Surfaces. *Planta* **1997**, *202*, 1–8.
6. Gao, L.; McCarthy, T. J. The "Lotus Effect" Explained: Two Reasons Why Two Length Scales of Topography Are Important. *Langmuir* **2006**, *22*, 2966–2967.
7. Ruibal, R.; Ernst, V. The Structure of the Digital Setae of Lizards. *J. Morph.* **1965**, *117*, 271–294.
8. Gao, H. J.; Wang, X.; Yao, H. M.; Gorb, S.; Arzt, E. Mechanics of Hierarchical Adhesion Structures of Geckos. *Mech. Mater.* **2005**, *37*, 275–285.
9. Kim, T. W.; Bhushan, B. Adhesion Analysis of Multi-Level Hierarchical Attachment System Contacting with a Rough Surface. *J. Adhes. Sci. Technol.* **2007**, *21*, 1–20.
10. Kim, T. W.; Bhushan, B. Effect of Stiffness of Multi-Level Hierarchical Attachment System on Adhesion Enhancement. *Ultramicroscopy* **2007**, *107*, 902–912.
11. Bhushan, B.; Jung, Y. C.; Koch, K. Micro-, Nano- and Hierarchical Structures for Superhydrophobicity, Self-Cleaning and Low Adhesion. *Philos. Trans. R. Soc. A* **2009**, *367*, 1631–1672.
12. Bhushan, B.; Jung, Y. C. Natural and Biomimetic Artificial Surfaces for Superhydrophobicity, Self-Cleaning, Low Adhesion, and Drag Reduction. *Prog. Mater. Sci.* **2011**, *56*, 1–108.
13. Verho, T.; Bower, C.; Andrew, P.; Franssila, S.; Ikkala, O.; Ras, R. H. A. Mechanically Durable Superhydrophobic Surfaces. *Adv. Mater.* **2011**, *23*, 673–678.
14. Sun, T.; Feng, L.; Gao, X.; Jiang, L. Bioinspired Surfaces with Special Wettability. *Acc. Chem. Res.* **2005**, *38*, 644–652.
15. Ma, M.; Gupta, M.; Li, Z.; Zhai, L.; Gleason, K. K.; Cohen, R. E.; Rubner, M. F.; Rutledge, G. C. Decorated Electrospun Fibers Exhibiting Superhydrophobicity. *Adv. Mater.* **2007**, *19*, 255–259.
16. Ma, M.; Hill, R. M.; Rutledge, G. C. A Review of Recent Results on Superhydrophobic Materials Based on Micro- and Nanofibers. *J. Adhes. Sci. Technol.* **2008**, *22*, 1799–1817.
17. Lin, J.; Cai, Y.; Wang, X.; Ding, B.; Yu, J.; Wang, M. Fabrication of Biomimetic Superhydrophobic Surfaces Inspired by Lotus Leaf and Silver Ragwort Leaf. *Nanoscale* **2011**, *3*, 1258–1262.
18. Kustandi, T. S.; Samper, V. D.; Ng, W. S.; Chong, A. S.; Gao, H. Fabrication of a Gecko-like Hierarchical Fibril Array Using a Bonded Porous Alumina Template. *J. Micromech. Microeng.* **2007**, *17*, N75–N81.
19. Greiner, C.; Arzt, E.; del Campo, A. Hierarchical Gecko-like Adhesives. *Adv. Mater.* **2009**, *21*, 479–482.
20. Murphy, M. P.; Kim, S.; Sitti, M. Enhanced Adhesion by Gecko-Inspired Hierarchical Fibrillar Adhesives. *ACS Appl. Mater. Interfaces* **2009**, *1*, 849–855.
21. Jeong, H. E.; Lee, J.-K.; Kim, H. N.; Moon, S. H.; Suh, K. Y. A Nontransferring Dry Adhesive with Hierarchical Polymer Nanohairs. *Proc. Natl. Acad. Sci. U.S.A.* **2009**, *106*, 5639–5644.
22. Ho, A. Y. Y.; Yeo, L. P.; Lam, Y. C.; Rodriguez, I. Fabrication and Analysis of Gecko-Inspired Hierarchical Polymer Nanosetae. *ACS Nano* **2011**, *5*, 1897–1906.
23. Matsen, M. W.; Schick, M. Stable and Unstable Phases of a Diblock Copolymer Melt. *Phys. Rev. Lett.* **1994**, *72*, 2660–2663.
24. Epps, T. H., III; Cochran, E. W.; Hardy, C. M.; Bailey, T. S.; Waletzko, R. S.; Bates, F. S. Network Phases in ABC Triblock Copolymers. *Macromolecules* **2004**, *37*, 7085–7088.
25. Chung, H.-j.; Ohno, K.; Fukuda, T.; Composto, R. J. Self-Regulated Structures in Nanocomposites by Directed Nanoparticle Assembly. *Nano Lett.* **2005**, *5*, 1878–1882.
26. Kim, B. J.; Fredrickson, G. H.; Hawker, C. J.; Kramer, E. J. Nanoparticle Surfactants as a Route to Bicontinuous Block Copolymer Morphologies. *Langmuir* **2007**, *23*, 7804–7809.
27. Meuler, A. J.; Hillmyer, M. A.; Bates, F. S. Ordered Network Mesostructures in Block Polymer Materials. *Macromolecules* **2009**, *42*, 7221–7250.
28. Hillmyer, M. A. Nanoporous Materials from Block Copolymer Precursors. *Adv. Polym. Sci.* **2005**, *190*, 137–181.
29. Olson, D. A.; Chen, L.; Hillmyer, M. A. Templating Nanoporous Polymers with Ordered Block Copolymers. *Chem. Mater.* **2008**, *20*, 869–890.
30. Ying, J. Y. Nanostructural Tailoring: Opportunities for Molecular Engineering in Catalysis. *AIChE J.* **2000**, *46*, 1902–1906.
31. Jackson, E. A.; Hillmyer, M. A. Nanoporous Membranes Derived from Block Copolymers: From Drug Delivery to Water Filtration. *ACS Nano* **2010**, *4*, 3548–3553.
32. Haberkorn, N.; Lechmann, M. C.; Sohn, B. H.; Char, K.; Gutmann, J. S.; Theato, P. Templated Organic and Hybrid Materials for Optoelectronic Applications. *Macromol. Rapid Commun.* **2009**, *30*, 1146–1166.
33. Hayakawa, T.; Horiuchi, S. From Angstroms to Micrometers: Self-Organized Hierarchical Structure within a Polymer Film. *Angew. Chem., Int. Ed.* **2003**, *42*, 2285–2289.
34. Ikkala, O.; ten Brinke, G. Hierarchical Self-Assembly in Polymeric Complexes: Towards Functional Materials. *Chem. Commun.* **2004**, 2131–2137.
35. ten Brinke, G.; Ruokolainen, J.; Ikkala, O. Supramolecular Materials Based on Hydrogen-Bonded Polymers. *Adv. Polym. Sci.* **2007**, *207*, 113–177.
36. Valkama, S.; Nykanen, A.; Kosonen, H.; Ramani, R.; Tuomisto, F.; Engelhardt, P.; ten Brinke, G.; Ikkala, O.; Ruokolainen, J. Hierarchical Porosity in Self-Assembled Polymers: Post-Modification of Block Copolymer—Phenolic Resin Complexes by Pyrolysis Allows the Control of Micro- and Mesoporosity. *Adv. Funct. Mater.* **2007**, *17*, 183–190.
37. Matsushita, Y. Creation of Hierarchically Ordered Nanophase Structures in Block Polymers Having Various Competing Interactions. *Macromolecules* **2007**, *40*, 771–776.
38. Hammond, M. R.; Mezzenga, R. Supramolecular Routes towards Liquid Crystalline Side-Chain Polymers. *Soft Matter* **2008**, *4*, 952–961.
39. Li, C.; Schlüter, A. D.; Zhang, A.; Mezzenga, R. A New Level of Hierarchical Structure Control by Use of Supramolecular Self-Assembled Dendronized Block Copolymers. *Adv. Mater.* **2008**, *20*, 4530–4534.
40. Tenneti, K. K.; Chen, X.; Li, C. Y.; Wan, X.; Fan, X.; Zhou, Q.-F.; Rong, L.; Hsiao, B. S. Competition between Liquid Crystallinity and Block Copolymer Self-Assembly in Core−Shell Rod−Coil Block Copolymers. *Soft Matter* **2008**, *4*, 458–461.
41. Hammond, M. R.; Li, C.; Tsitsilianis, C.; Mezzenga, R. Hierarchical Self-Organization in Polyelectrolyte−Surfactant Complexes Based on Heteroarm Star Block Copolyampholytes. *Soft Matter* **2009**, *5*, 2371–2377.
42. Bolognesi, A.; Galeotti, F.; Giovanella, U.; Bertini, F.; Yunus, S. Nanophase Separation in Polystyrene−Polyfluorene Block Copolymers Thin Films Prepared through the Breath Figure Approach. *Langmuir* **2009**, *25*, 5333–5338.
43. Muñoz-Bonilla, A.; Ibarboure, E.; Papon, E.; Rodriguez-Hernandez, J. Self-Organized Hierarchical Structures in Polymer Surfaces: Self-Assembled Nanostructures within Breath Figures. *Langmuir* **2009**, *25*, 6493–6499.
44. Matsushita, Y.; Takano, A.; Hayashida, K.; Asari, T.; Noro, A. Hierarchical Nanophase-Separated Structures Created by Precisely-Designed Polymers with Complexity. *Polymer* **2009**, *50*, 2191–2203.
45. Chen, X.-F.; Shen, Z.; Wan, X.-H.; Fan, X.-H.; Chen, E.-Q.; Ma, Y.; Zhou, Q.-F. Mesogen-Jacketed Liquid Crystalline Polymers. *Chem. Soc. Rev.* **2010**, *39*, 3072–3101.

46. Hu, D.; Xu, Z.; Zeng, K.; Zheng, S. From Self-Organized Novolac Resins to Ordered Nanoporous Carbons. *Macromolecules* **2010**, *43*, 2960–2969.
47. Escalé, P.; Save, M.; Lapp, A.; Rubatat, L.; Billon, L. Hierarchical Structures Based on Self-Assembled Diblock Copolymers within Honeycomb Micro-structured Porous Films. *Soft Matter* **2010**, *6*, 3202–3210.
48. Escalé, P.; Rubatat, L.; Derail, C.; Save, M.; Billon, L. pH Sensitive Hierarchically Self-Organized Bioinspired Films. *Macromol. Rapid Commun.* **2011**, *32*, 1072–1076.
49. Stewart-Sloan, C. R.; Thomas, E. L. Interplay of Symmetries of Block Polymers and Confining Geometries. *Eur. Polym. J.* **2011**, *47*, 630–646.
50. Wu, Y.; Cheng, G.; Katsov, K.; Sides, S. W.; Wang, J.; Tang, J.; Fredrickson, G. H.; Moskovits, M.; Stucky, G. D. Composite Mesostructures by Nano-confinement. *Nat. Mater.* **2004**, *3*, 816–822.
51. Xiang, H.; Shin, K.; Kim, T.; Moon, S. I.; McCarthy, T. J.; Russell, T. P. Block Copolymers under Cylindrical Confinement. *Macromolecules* **2004**, *37*, 5660–5664.
52. Shin, K.; Xiang, H.; Moon, S. I.; Kim, T.; McCarthy, T. J.; Russell, T. P. Curving and Frustrating Flatland. *Science* **2004**, *306*, 76.
53. Xiang, H.; Shin, K.; Kim, T.; Moon, S. I.; McCarthy, T. J.; Russell, T. P. From Cylinders to Helices upon Confinement. *Macromolecules* **2005**, *38*, 1055–1056.
54. Xiang, H.; Shin, K.; Kim, T.; Moon, S.; McCarthy, T. J.; Russell, T. P. The Influence of Confinement and Curvature on the Morphology of Block Copolymers. *J. Polym. Sci., Part B: Polym. Phys.* **2005**, *43*, 3377–3383.
55. Sun, Y.; Steinhart, M.; Zschech, D.; Adhikari, R.; Michler, G. H.; Gösele, U. Diameter-Dependence of the Morphology of PS-*b*-PMMA Nanorods Confined within Ordered Porous Alumina Templates. *Macromol. Rapid Commun.* **2005**, *26*, 369–375.
56. Wang, Y.; Gösele, U.; Steinhart, M. Mesoporous Polymer Nanofibers by Infiltration of Block Copolymers with Sacrificial Domains into Porous Alumina. *Chem. Mater.* **2008**, *20*, 379–381.
57. Wang, Y.; Gösele, U.; Steinhart, M. Mesoporous Block Copolymer Nanorods by Swelling-Induced Morphology Reconstruction. *Nano Lett.* **2008**, *8*, 3548–3553.
58. Dobriyal, P.; Xiang, H.; Kazuyuki, M.; Chen, J.-T.; Jinnai, H.; Russell, T. P. Cylindrically Confined Diblock Copolymers. *Macromolecules* **2009**, *42*, 9082–9088.
59. Wang, Y.; Qin, Y.; Berger, A.; Yau, E.; He, C.; Zhang, L.; Gösele, U.; Knez, M.; Steinhart, M. Nanoscopic Morphologies in Block Copolymer Nanorods as Templates for Atomic-Layer Deposition of Semiconductors. *Adv. Mater.* **2009**, *21*, 2763–2766.
60. Jeon, S.-M.; Lee, Y.; Kim, J.-H.; Lee, J.-K.; Char, K.; Sohn, B.-H. Internal Morphologies of Diblock Copolymer Nanorods Fabricated from Regular and Irregular Pores of Anodized Aluminum Oxide Templates. *React. Funct. Polym.* **2009**, *69*, 558–563.
61. Chen, D.; Park, S.; Chen, J.-T.; Redston, E.; Russell, T. P. A Simple Route for the Preparation of Mesoporous Nanostructures Using Block Copolymers. *ACS Nano* **2009**, *3*, 2827–2833.
62. Pulamagatta, B.; Yau, M. Y. E.; Gunkel, I.; Thurn-Albrecht, T.; Schröter, K.; Pfefferkorn, D.; Kressler, J.; Steinhart, M.; Binder, W. H. Block Copolymer Nanotubes by Melt-Infiltration of Nanoporous Aluminum Oxide. *Adv. Mater.* **2011**, *23*, 781–786.
63. Wang, Y.; Tong, L.; Steinhart, M. Swelling-Induced Morphology Reconstruction in Block Copolymer Nanorods: Kinetics and Impact of Surface Tension During Solvent Evaporation. *ACS Nano* **2011**, *5*, 1928–1938.
64. Li, F.; Zhang, L.; Metzger, R. M. On the Growth of Highly Ordered Pores in Anodized Aluminum Oxide. *Chem. Mater.* **1998**, *10*, 2470–2480.
65. Lee, W.; Ji, R.; Gösele, U.; Nielsch, K. Fast Fabrication of Long-Range Ordered Porous Alumina Membranes by Hard Anodization. *Nat. Mater.* **2006**, *5*, 741–747.
66. Kalra, V.; Mendez, S.; Lee, J. H.; Nguyen, H.; Marquez, M.; Joo, Y. L. Confined Assembly in Coaxially Electrospun Block Copolymer Fibers. *Adv. Mater.* **2006**, *18*, 3299–3303.
67. Ma, M.; Krikorian, V.; Yu, J. H.; Thomas, E. L.; Rutledge, G. C. Electrospun Polymer Nanofibers with Internal Periodic Structure Obtained by Microphase Separation of Cylindrically Confined Block Copolymers. *Nano Lett.* **2006**, *6*, 2969–2972.
68. Kalra, V.; Lee, J.; Lee, J. H.; Lee, S. G.; Marquez, M.; Wiesner, U.; Joo, Y. L. Controlling Nanoparticle Location *via* Confined Assembly in Electrospun Block Copolymer Nanofibers. *Small* **2008**, *4*, 2067–2073.
69. Kalra, V.; Lee, J. H.; Park, J. H.; Marquez, M.; Joo, Y. L. Confined Assembly of Asymmetric Block-Copolymer Nanofibers *via* Multiaxial Jet Electrospinning. *Small* **2009**, *5*, 2323–2332.
70. Ma, M.; Titievsky, K.; Thomas, E. L.; Rutledge, G. C. Continuous Concentric Lamellar Block Copolymer Nanofibers with Long Range Order. *Nano Lett.* **2009**, *9*, 1678–1683.
71. Ma, M.; Thomas, E. L.; Rutledge, G. C.; Yu, B.; Li, B.; Jin, Q.; Ding, D.; Shi, A.-C. Gyroid-Forming Diblock Copolymers Confined in Cylindrical Geometry: A Case of Extreme Makeover for Domain Morphology. *Macromolecules* **2010**, *43*, 3061–3071.
72. Kamperman, M.; Korley, L. T. J.; Yau, B.; Johansen, K. M.; Joo, Y. L.; Wiesner, U. Nanomanufacturing of Continuous Composite Nanofibers with Confinement-Induced Morphologies. *Polym. Chem.* **2010**, *1*, 1001–1004.
73. Yabu, H.; Higuchi, T.; Shimomura, M. Unique Phase-Separation Structures of Block-Copolymer Nanoparticles. *Adv. Mater.* **2005**, *17*, 2062–2065.
74. Higuchi, T.; Tajima, A.; Motoyoshi, K.; Yabu, H.; Shimomura, M. Frustrated Phases of Block Copolymers in Nanoparticles. *Angew. Chem., Int. Ed.* **2008**, *47*, 8044–8046.
75. Li, L.; Matsunaga, K.; Zhu, J.; Higuchi, T.; Yabu, H.; Shimomura, M.; Jinnai, H.; Hayward, R. C.; Russell, T. P. Solvent-Driven Evolution of Block Copolymer Morphology under 3D Confinement. *Macromolecules* **2010**, *43*, 7807–7812.
76. Okubo, M.; Saito, N.; Takekoh, R.; Kobayashi, H. Morphology of Polystyrene/Polystyrene-*block*-Poly(methyl methacrylate)/Poly(methyl methacrylate) Composite Particles. *Polymer* **2005**, *46*, 1151–1156.
77. Tanaka, T.; Saito, N.; Okubo, M. Control of Layer Thickness of Onionlike Multilayer Composite Polymer Particles Prepared by the Solvent Evaporation Method. *Macromolecules* **2009**, *42*, 7423–7429.
78. Bates, F. S.; Maurer, W. W.; Lipic, P. M.; Hillmyer, M. A.; Almdal, K.; Mortensen, K.; Fredrickson, G. H.; Lodge, T. P. Polymeric Bicontinuous Microemulsions. *Phys. Rev. Lett.* **1997**, *79*, 849–852.
79. Hillmyer, M. A.; Maurer, W. W.; Lodge, T. P.; Bates, F. S.; Almdal, K. Model Bicontinuous Microemulsions in Ternary Homopolymer/Block Copolymer Blends. *J. Phys. Chem. B* **1999**, *103*, 4814–4824.
80. Jones, B. H.; Lodge, T. P. High-Temperature Nanoporous Ceramic Monolith Prepared from a Polymeric Bicontinuous Microemulsion Template. *J. Am. Chem. Soc.* **2009**, *131*, 1676–1677.
81. Jones, B. H.; Lodge, T. P. Nanoporous Materials Derived from Polymeric Bicontinuous Microemulsions. *Chem. Mater.* **2010**, *22*, 1279–1281.
82. Jones, B. H.; Lodge, T. P. Hierarchically Porous Silica Prepared from Ionic Liquid and Polymeric Bicontinuous Microemulsion Templates. *Chem. Mater.* **2011**, in press.
83. Fleury, G.; Bates, F. S. Hierarchically Structured Bicontinuous Polymeric Microemulsions. *Soft Matter* **2010**, *6*, 2751–2759.
84. Arsenault, A. C.; Rider, D. A.; Tétreault, N.; Chen, J. I.-L.; Coombs, N.; Ozin, G. A.; Manners, I. Block Copolymers under Periodic, Strong Three-Dimensional Confinement. *J. Am. Chem. Soc.* **2005**, *127*, 9954–9955.
85. Rider, D. A.; Chen, J. I. L.; Eloi, J.-C.; Arsenault, A. C.; Russell, T. P.; Ozin, G. A.; Manners, I. Controlling the Morphologies of Organometallic Block Copolymers in the 3-Dimensional Spatial Confinement of Colloidal and Inverse Colloidal Crystals. *Macromolecules* **2008**, *41*, 2250–2259.

86. Fu, J.; Wang, J.; Li, Q.; Kim, D. H.; Knoll, W. 3D Hierarchically Ordered Composite Block Copolymer Hollow Sphere Arrays by Solution Wetting. *Langmuir* **2010**, *26*, 12336–12341.
87. Yabu, H.; Jinno, T.; Koike, K.; Higuchi, T.; Shimomura, M. Three-Dimensional Assembly of Gold Nanoparticles in Spherically Confined Microphase-Separation Structures of Block Copolymers. *Macromolecules* **2011**, *44*, 5868–5873.
88. Jones, B. H.; Cheng, K.-Y.; Holmes, R. J.; Lodge, T. P. Nanoporous Polyethylene Thin Films Templated by Polymeric Bicontinuous Microemulsions: Evolution of Morphology on Non-neutral Substrates. *ACS Appl. Mater. Interf.* **2011**, DOI: 10.1021/am2009794.
89. Barrett, E. P.; Joyner, L. G.; Halenda, P. P. The Determination of Pore Volume and Area Distributions in Porous Substances. I. Computations from Nitrogen Isotherms. *J. Am. Chem. Soc.* **1951**, *73*, 373–380.
90. Fetters, L. J.; Lohse, D. J.; Richter, D.; Witten, T. A.; Zirkel, A. Connection between Polymer Molecular Weight, Density, Chain Dimensions, and Melt Viscoelastic Properties. *Macromolecules* **1994**, *27*, 4639–4647.
91. Gehlsen, M. D.; Weimann, P. A.; Bates, F. S.; Harville, S.; Mays, J. W.; Wignall, G. D. Synthesis and Characterization of Poly(vinylcyclohexane) Derivatives. *J. Polym. Sci., Part B: Polym. Phys.* **1995**, *33*, 1527–1536.
92. Hückstädt, H.; Goldacker, T.; Göpfert, A.; Abetz, V. Core−Shell Double Gyroid Morphologies in ABC Triblock Copolymers with Different Chain Topologies. *Macromolecules* **2000**, *33*, 3757–3761.
93. Kimishima, K; Jinnai, H.; Hashimoto, T. Control of Self-Assembled Structures in Binary Mixtures of A−B Diblock Copolymer and A−C Diblock Copolymer by Changing the Interaction between B and C Block Chains. *Macromolecules* **1999**, *32*, 2585–2596.
94. Funaki, Y.; Kumano, K.; Nakao, T.; Jinnai, H.; Yoshida, H.; Kimishima, K.; Tsutsumi, K.; Hirokawa, Y.; Hashimoto, T. Influence of Casting Solvents on Microphase-Separated Structures of Poly(2-vinylpyridine)-*block*-Polyisoprene. *Polymer* **1999**, *40*, 7147–7156.
95. Park, I.; Park, S.; Park, H.-W.; Chang, T.; Yang, H.; Ryu, C. Y. Unexpected Hexagonally Perforated Layer Morphology of PS-*b*-PMMA Block Copolymer in Thin Supported Film. *Macromolecules* **2006**, *39*, 315–318.
96. Teubner, M.; Strey, R. Origin of the Scattering Peak in Microemulsions. *J. Chem. Phys.* **1987**, *87*, 3195–3200.
97. Lee, M. N.; Mohraz, A. Bicontinuous Macroporous Materials from Bijel Templates. *Adv. Mater.* **2010**, *22*, 4836–4841.
98. Lee, M. N.; Mohraz, A. Hierarchically Porous Silver Monoliths from Colloidal Bicontinuous Interfacially Jammed Emulsion Gels. *J. Am. Chem. Soc.* **2011**, *133*, 6945–6947.
99. Gu, Y.; Huang, J. Fabrication of Natural Cellulose Substance Derived Hierarchical Polymeric Materials. *J. Mater. Chem.* **2009**, *19*, 3764–3770.
100. Zou, C.; Wu, D.; Li, M.; Zeng, Q.; Xu, F.; Huang, Z.; Fu, R. Template-Free Fabrication of Hierarchical Porous Carbon by Constructing Carbonyl Crosslinking Bridges between Polystyrene Chains. *J. Mater. Chem.* **2010**, *20*, 731–735.
101. Choi, S.-H.; Bates, F. S.; Lodge, T. P. Structure of Poly(styrene-*b*-ethylene-*alt*-propylene) Diblock Copolymer Micelles in Squalane. *J. Phys. Chem. B* **2009**, *113*, 13840–13848.
102. Cavicchi, K. A.; Lodge, T. P. Self-Diffusion and Tracer Diffusion in Sphere-Forming Block Copolymers. *Macromolecules* **2003**, *36*, 7158–7164.
103. Cavicchi, K. Diffusion in Cylinder and Sphere-Forming Block Copolymers. Ph.D. Thesis, University of Minnesota, 2003.
104. Ren, Y.; Lodge, T. P.; Hillmyer, M. A. Synthesis, Characterization, and Interaction Strengths of Difluorocarbene-Modified Polystyrene-Polyisoprene Block Copolymers. *Macromolecules* **2000**, *33*, 866–876.
105. Bellas, V.; Iatrou, H.; Pitsinos, E. N.; Hadjichristidis, N. Heterofunctional Linking Agents for the Synthesis of Well-Defined Block Copolymers of Dimethylsiloxane and *tert*-Butyl Methacrylate or 2-Vinylpridine. *Macromolecules* **2001**, *34*, 5376–5378.
106. Huglin, M. B. *Light Scattering from Polymer Solutions*; Academic Press: New York, 1972.
107. Saito, R.; Kotsubo, H.; Ishizu, K. Synthesis of Microspheres with `Hairy-Ball' Structures from Poly(styrene-*b*-2-vinyl pyridine) Diblock Copolymers. *Polymer* **1992**, *33*, 1073–1077.
108. Okumura, A.; Nishikawa, Y.; Hashimoto, T. Nano-Fabrication of Double Gyroid Network Structure *via* Ozonolysis of Matrix Phase of Polyisoprene in Poly(2-vinylpyridine)-*block*-Polyisoprene Films. *Polymer* **2006**, *47*, 7805–7812.